Silicon Nitride Interferometers for Optical Sensing with Multi-micron Dimensions

Silicon Nitride Interferometers for Optical Sensing with Multi-micron Dimensions

João Costa[1,2], Daniel Almeida[1,2,3], Alessandro Fantoni[1,2], Paulo Lourenço[1,2,3], Manuela Vieira[1,2,3]

[1]ISEL - Instituto Superior de Engenharia de Lisboa, Instituto Politécnico de Lisboa, Lisboa, Portugal
[2]UNINOVA-CTS, Caparica, Portugal
[3]School of Science and Technology, NOVA University of Lisbon, Caparica, Portugal
jcosta@deetc.isel.ipl.pt

Abstract. Increasing the size of the smallest features of Photonic Integrated Circuits (PICs) to multi-micron dimensions can be advantageous to avoid expensive and complex lithographic steps in the fabrication process. In applications where extremely reduced chip size is not a requirement, the design of devices with multi-micron dimensions is potential interesting to avoid the need for e-beam lithography. Another benefit is that making the dimensions larger reduces the effect of lithographic imperfections such as waveguide surface roughness. However, the benefits do not come without limitations. Coupling the light in and out of the circuit is more challenging since diffraction gratings are not available when designing for such large dimensions. Circuit bends must have a larger radius of curvature and the existence of multimode propagation conditions can have detrimental impact in the performance of several devices, such as interferometers. In this study we perform simulations of the coupling between a lensed multimode optical fiber and a multi-micron a-SiN:H rib waveguide. Light coupling efficiency is analyzed as a function of distance variations using the FDTD method and compared with coupling to a strip waveguide. Moreover, we use numerical simulations to study the performance of a Mach-Zehnder interferometer sensitive to refractive index variations. Both the interferometer, splitters and combiners are designed with multi-micron dimensions.

Keywords: multi-micron, rib waveguides, interferometers, splitters, combiners

1. Introduction

Photonic devices with features above the micrometer have advantages over their sub-micrometer counterparts. Notably, the less demanding optical lithographic process, based on ultraviolet wavelengths is less expensive when compared with electron beam lithography. In addition multi-micron waveguides can achieve much lower attenuation [1] and are less affected by side-wall roughness, as demonstrated by Lee *et al.* [2].

There are several methods that can be applied to couple light into waveguides, being typically based on vertical and horizontal tapers [3]–[5], wedges [6], prisms [7], [8], diffraction gratings [7], [9] and end-fire coupling [7], [10]. To avoid the inclusion of complex structures, which require expensive and high-resolution fabrication methods, end-fire coupling was the method selected in this study. Light is coupled to the waveguide by means of an optical fiber terminated by a plano-convex lens.

In the context of this work rib waveguides are an attractive solution because single mode propagation can be achieved for larger dimensions, when compared with strip waveguides. Some of the most common beam splitting and combining devices/strategies rely on Y-junctions [11], [12], S-bends [12],

coupled mode [12]–[14] or multi-mode interference (MMI) [12], [15]–[17]. Another technique often applied in rib waveguides due to its compactness, is based on trenches filled with a dielectric medium (e.g., air, SU-8), which act as mirrors and can find applications in light distribution, by employing a T-shaped branch geometry [12], [18]. Due to its lower complexity and fabrication expenses, in this study we devised a light distribution technique based on multi-mode interference, including tapered access waveguides [19]. These devices are etched directly in the amorphous silicon nitride (a-SiN:H) layer, avoiding the need for a supplementary lithographic mask, thus minimizing production costs.

Changing the beam propagation route is more challenging in rib waveguides, several techniques can be applied to guide light in a different direction with minimal losses, like for example: a) circumference arc-based curves, which typically have a very large radius on the mm range [20]–[23]; b) curves/bends based on non-linear functions (e.g., spline) [24], [25], these can typically be made more compact than arc-based curves; c) dielectric filled trenches (e.g. air or SU-8 trenches) [26], [27].

In this article we use numerical simulations to study the performance of a multi-micron Mach-Zehnder interferometer sensitive to refractive index variations in the layer covering the test and reference arms. The device is designed for an operation wavelength of 633 nm.

2. Design and Methods

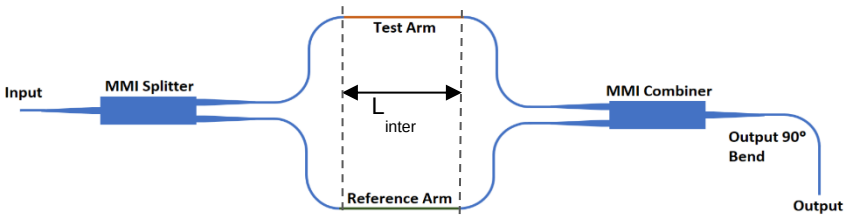

Figure 1 - Diagram showing the various components of the device.

Figure 1 presents a diagram of the device. The waveguide transversal section, as illustrated in

Figure 2, corresponds to the dimensions of the input, output, and interferometer segments. Large values for the height (H=1.2 µm) and width (w=2 µm) were defined but still within the single mode conditions for the rib waveguide as proposed by Soref *et al*. [28]. The waveguides are made of hydrogenated amorphous silicon nitride (a-SiN:H), with refractive index n=1.92 and having a glass substrate with n=1.51 as depicted in

Figure 2. Adiabatic tappers of length 60 µm have been used at the input and output of the splitters and combiners to improve their performance [19]. The wider end of the tappers was set to 6 µm. Since the light source and photodetector are in the horizontal plane, a 90º waveguide bend is required to prevent direct illumination of the photodetector. Furthermore, the bend attenuates higher order modes and prevents light leaked from the combiner to reach the photodetector, as described in the results section.

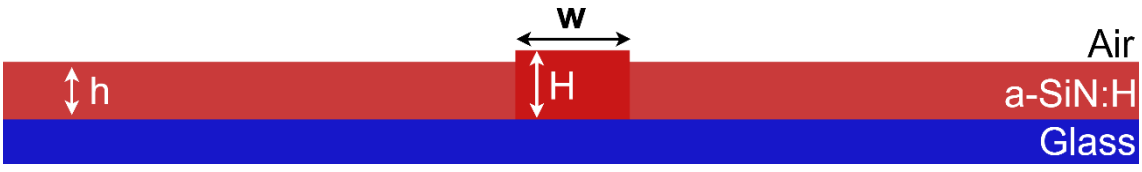

Figure 2 - Transversal section of the proposed rib waveguide, showing design parameters (rib width w=2 µm, slab height h=1 µm and rib height H=1.2 µm).

In order to emulate the input light beam the launch field was defined as the fundamental mode of an optical fiber with diameter 19.4 µm fitted with an output lens. The lens center thickness is 1.55 µm and the diameter the same as the fiber. Light propagates through the lens and on a short free space region before reaching the input waveguide as displayed in Figure 3. Simulations were performed in 3-D using the Finite Difference Time Domain (FDTD) method and assuming quasi-TM polarization (major

electric field in vertical y direction). This polarization has the interesting property of potentially being able to excite surface plasmon polaritons, if the sensing region is covered with metal, which is a common approach in biosensing applications.

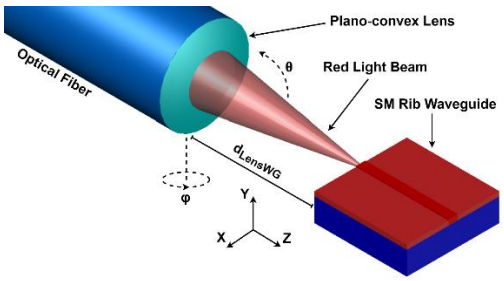

Figure 3 - Light coupling scheme employing a lensed optical fiber, terminated by a plano-convex lens. The Euclidean space axis (X, Y, Z), the rotation and elevation angles of the optical fiber (ϕ and Θ, respectively) are represented. For better visualization the figure is not up to scale.

The splitter and combiner are 24 μm wide and 868 μm long. The length was optimized by numerical simulations using the Fully Vectorial Beam Propagation Method (FV-BPM), as implemented in the software package Rsoft (Synopsys Inc.).

The sensing region consist of two arms where the samples are placed. One of the arms contains the reference sample, water, and the other a test sample, e.g. glycerol. The length of the sensing region, L_{inter}, is set to achieve phase opposition for a specific target sample.

$$L_{inter} = \frac{\lambda_0}{2\Delta n_{eff}}, \qquad Eq.\ 1$$

where λ_0=633 nm is the free space wavelength (μm) and Δn_{eff} is the effective refractive index difference of the modes propagating on the reference and testing arms. Numerical Simulations using the Finite Element Approach (FemSIM, Rsoft, Synopsys Inc.) were used to calculate the effective indexes. As an example, for this study, we obtained L_{inter} = 860 μm when using glycerol as the target analyte and water as the reference sample.

3. Results

The overlap between the fundamental quasi-TM mode of the waveguide and the input light beam is presented in Figure 4a. We observe that the coupling efficiency is dependent on the distance between the lensed fiber and the input waveguide, as expected, achieving a minimum coupling loss of 3.2 dB at a distance of 33.45 μm. For comparison, we made the same study with a single mode strip waveguide 0.4 μm wide and 0.2μm thick. Results of the study are presented in Figure 4b, the coupling loss is approximately 7.9 dB for the optimized distance, about 4.7 dB higher than the loss achievable with the rib waveguide geometry.

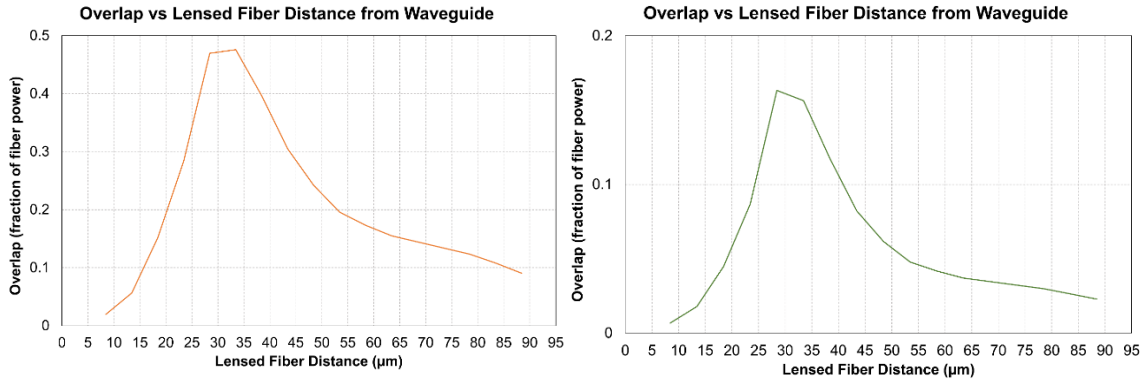

(a) (b)

Figure 4 - Fundamental quasi-TM mode overlap as a function of distance between lensed optical fiber and the waveguide's input. Subfigure (a) presents coupling to a single mode rib waveguide and (b) to a single mode strip waveguide.

Power overlaps consists in the fraction of power carried in the fundamental rib waveguide mode normalized to the input power. In what concerns the splitter, overlap in each output is -3.2 dB, which is near the ideal -3 dB for the 1x2 splitter. The intensity of the Ey field is displayed in Figure 5a showing the expected pattern with two strong peaks at the top of the figure, corresponding to the two output rib waveguides. A combiner, having the same dimensions as the splitter, only with inverse topology (2x1), combines the light from the two arms of the interferometer. Simulations in FV-BPM show that with in-phase inputs, the output overlap is -0.2 dB. Accordingly, Figure 5b shows a strong peak in the top center corresponding to the region of the output waveguide. With inputs in phase opposition the output overlap is -99 dB. In agreement, Figure 5c displays a dark region in the top central region, corresponding to a strong attenuation in this region.

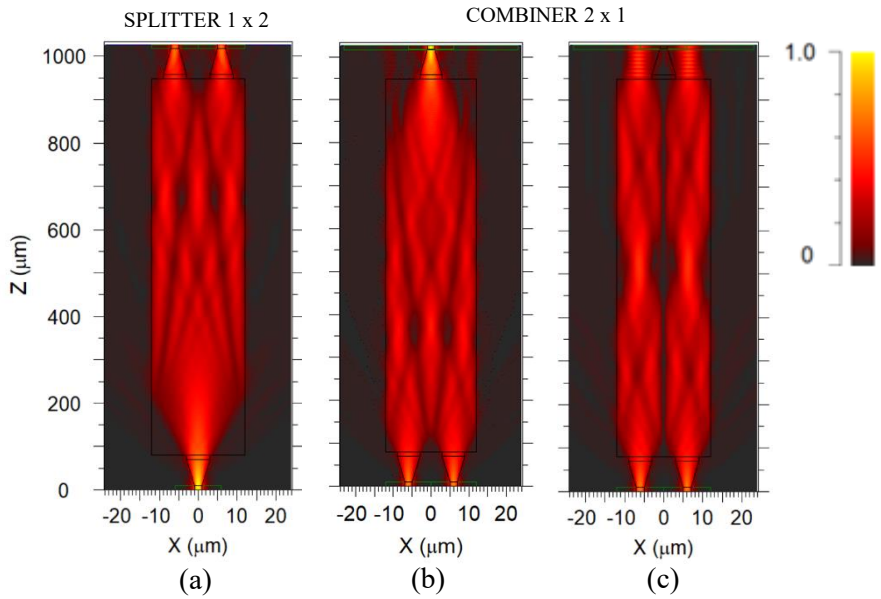

(a) (b) (c)

Figure 5 Intensity of the major Ey field in the Multi-Mode Interference devices. The input is located at the bottom in all subfigures: (a) 1x2 splitter; (b) 2x1 combiner with in-phase inputs; (c) 2x1 combiner with phase opposition inputs.

The waveguide bend attenuates higher order modes, directing only the signal in the combiner's output waveguide to the photodetector. Simulations with SV-BPM were performed for a 3 mm curvature radius.

Table 1 – Power attenuation after the 90º bend

Field before 90º Bend	**Power Attenuation after 90º Bend**
Quasi TM00 (fundamental mode)	0.1 dB
Quasi TM01 (higher order mode)	20.3 dB
Quasi TM02 (higher order mode)	32.0 dB

In Table 1 we can see the results from simulations. The fundamental mode is only slightly attenuated by the 90º bend, 0.1dB, whereas higher order modes experience attenuations of over 20 dB. In other words, non-ideal effects caused by the eventual presence of higher order modes are minimized by the bend.

The overlap is not the most adequate parameter to evaluate performance since light leakage from the combiner is very significant as can be noticed in Figure 5c. To overcome this issue the power transmitted following the 90º bend was determined which is directly related to the power received by the photodetector. When considering the combiner plus the 90º bend we obtained over 16 dB difference in transmitted power between in-phase and out of phase signals originated in the interferometer.

The length of the interferometer was adjusted to obtain maximum sensitivity when sampling glycerol (n=1.47), as previously described. At this index of refraction, we obtained a sensitivity of 355 dB/RIU from numerical simulations. The limit of detection is dependent on the noise of the optoelectronic system, if the system can measure changes in optical power of 0.01 dB, variations in the refractive index as small as 2.8×10^{-5} RIU can be detected. However special attention should be given to the effect of temperature when targeting small limits of detection. The thermo-optic coefficient of silicon nitride is dependent on temperature, wavelength, and silicon content of the film produced [29]. At room temperature and wavelengths 600-800 nm, thermo-optic coefficients have been reported in the range 10^{-5} to 10^{-4} K^{-1} [30]. In addition, the reference sample may also display refractive index variation with temperature, for example the thermo-optic coefficient of water is of the order 10^{-4} K^{-1} at 25 °C [31]. Hence, when constant temperature measurements are not possible it is necessary to perform a more in-depth study of thermo-optic factors to determine the limit of detection.

4. Conclusions

Multi-micron a-SiN:H interferometers for refractive index sensing were designed based on rib waveguides with lithographic features no smaller than 2 μm. As proof-of-concept numerical simulations with glycerol and water as the target and reference samples, respectively, show that by setting the length of the arms appropriately, a target sample can produce a power attenuation of more than 16 dB relative to the reference sample. This approach could be of interest to design low-cost refractive index sensors.

Acknowledgements

This research was supported by Instituto Politécnico de Lisboa through project IPL/2021/wavesensor_ISEL and IPL/2021/MuMiAS 2D_ISEL, and by FCT – Fundação para a Ciência e Tecnologia through grants SFRH/BD/07792/2021, SFRH/BD/144833/2019, PTDC/NAN-OPT/31311/2017 and FCT/MCTES: UIDB/00066/2020.

References

[1] A. J. Zilkie *et al.*, "Multi-micron silicon photonics platform for highly manufacturable and versatile photonic integrated circuits," *IEEE J. Sel. Top. Quantum Electron.*, vol. 25, no. 5,

2019, doi: 10.1109/JSTQE.2019.2911432.
[2] K. K. Lee, D. R. Lim, H. C. Luan, A. Agarwal, J. Foresi, and L. C. Kimerling, "Effect of size and roughness on light transmission in a Si/SiO2 waveguide: Experiments and model," *Appl. Phys. Lett.*, vol. 77, no. 11, pp. 1617–1619, 2000, doi: 10.1063/1.1308532.
[3] D. Grajales, A. F. Gavela, C. Domínguez, J. R. Sendra, and L. M. Lechuga, "Low-cost vertical taper for highly efficient light in-coupling in bimodal nanointerferometric waveguide biosensors," *JPhys Photonics*, vol. 1, no. 2, 2019, doi: 10.1088/2515-7647/aafebb.
[4] M. Tokushima, H. Kawashima, T. Horikawa, and K. Kurata, "Post-Integrated Dual-Core Large-End Spot-Size Converter with Si Vertical Taper for Fiber Butt-Coupling to Si-Photonics Chip," *J. Light. Technol.*, vol. 36, no. 20, pp. 4783–4791, 2018, doi: 10.1109/JLT.2018.2863732.
[5] K. Shiraishi, R. Takasaki, H. Yoda, H. Oshikiri, and C. S. Tsai, "A Viable Spot-Size Converter for Coupling Between a Single-Mode Fiber and a Silicon-Wire Waveguide," in *2014 International Conference on Electronics Packaging (ICEP)*, 2014, pp. 799–802.
[6] J. Schrauwen, S. Scheerlinck, D. Van Thourhout, and R. Baets, "Polymer wedge for perfectly vertical light coupling to silicon," *Integr. Opt. Devices, Mater. Technol. XIII*, vol. 7218, no. 0, p. 72180B, 2009, doi: 10.1117/12.807558.
[7] E. Voges, "Coupling Techniques: Prism-, Grating- and Endfire-Coupling," *Integr. Opt. Springer, Boston, MA*, pp. 323–333, 1983.
[8] T. Tang, J. Qin, J. Xie, L. Deng, and L. Bi, "Magneto-optical Goos-Hänchen effect in a prism-waveguide coupling structure," *Opt. Express*, vol. 22, no. 22, p. 27042, 2014, doi: 10.1364/oe.22.027042.
[9] X. Chen, C. Li, C. K. Y. Fung, S. M. G. Lo, and H. K. Tsang, "Apodized waveguide grating couplers for efficient coupling to optical fibers," *IEEE Photonics Technol. Lett.*, vol. 22, no. 15, pp. 1156–1158, 2010, doi: 10.1109/LPT.2010.2051220.
[10] G. Son, S. Han, J. Park, K. Kwon, and K. Yu, "High-efficiency broadband light coupling between optical fibers and photonic integrated circuits," *Nanophotonics*, vol. 7, no. 12, pp. 1845–1864, 2018, doi: 10.1515/nanoph-2018-0075.
[11] D. Seyringer, J. Chovan, L. Gajdosova, D. Figura, and F. Uherek, "Comparison of silicon nitride based 1×8 Y-branch splitters applying different waveguide structures," *Int. Conf. Transparent Opt. Networks*, vol. 2019-July, pp. 17–20, 2019, doi: 10.1109/ICTON.2019.8840394.
[12] D. Yuan, Y. Dong, Y. Liu, and T. Li, "Mach-Zehnder interferometer biochemical sensor based on silicon-on-insulator rib waveguide with large cross section," *Sensors (Switzerland)*, vol. 15, no. 9, pp. 21500–21517, 2015, doi: 10.3390/s150921500.
[13] S. Samanta, P. K. Dey, P. Banerji, and P. Ganguly, "A 1×2 polarization-independent power splitter using three-coupled silicon rib waveguides," *J. Opt.*, vol. 20, no. 9, 2018.
[14] V. H. Nguyen, I. K. Kim, and T. J. Seok, "Low-Loss and Broadband Silicon Photonic 3-dB Power Splitter with Enhanced Coupling of Shallow-Etched Rib Waveguides," *Appl. Sci.*, vol. 10, no. 13, p. 4507, 2020.
[15] D. Kwong, Y. Zhang, A. Hosseini, Y. Z. Liu, and R. T. Chen, "Demonstration of rib waveguide based 1×12 multimode interference optical beam splitter on silicon-on-insulator," *2010 IEEE Photonics Soc. Summer Top. Meet. Ser. PHOSST 2010*, pp. 221–222, 2010, doi: 10.1109/PHOSST.2010.5553694.
[16] L. Vivien *et al.*, "Comparison between strip and rib SOI microwaveguides for intra-chip light distribution," *Opt. Mater. (Amst).*, vol. 27, no. 5, pp. 756–762, 2005, doi: 10.1016/j.optmat.2004.08.010.
[17] J. Costa, D. Almeida, A. Fantoni, P. Lourenco, M. Fernandes, and M. Vieira, "Performance of an a-Si:H MMI multichannel beam splitter analyzed by computer simulation," *Silicon Photonics XVI, SPIE*, vol. 1169106, 2021, doi: 10.1117/12.2583028.
[18] E. Cassan, S. Laval, S. Lardenois, and A. Koster, "On-Chip Optical Interconnects With

Compact and Low-Loss Light Distribution in Silicon-on-Insulator Rib Waveguides," *IEEE J. Sel. Top. Quantum Electron.*, vol. 9, no. 2, pp. 460–464, 2003, doi: 10.1109/IITC.2003.1219706.

[19] D. J. Thomson, Y. Hu, G. T. Reed, and J.-M. Fedeli, "Low loss MMI couplers for high performance MZI modulators," *IEEE Photonics Technol. Lett.*, vol. 22, no. 20, pp. 1485–1487, 2010, doi: 10.1109/LPT.2010.2063018.

[20] C. Yuanyuan, Y. Qingfeng, Y. Di, C. Shaowu, and Y. Jinzhong, "Structural optimizations of SOI-based single-mode rib waveguide bends," *Int. Conf. Solid-State Integr. Circuits Technol. Proceedings, ICSICT*, vol. 3, pp. 2015–2017, 2004, doi: 10.1109/icsict.2004.1435236.

[21] D. Dai and S. He, "Analysis of characteristics of bent rib waveguides," *J. Opt. Soc. Am. A*, vol. 21, no. 1, p. 113, 2004, doi: 10.1364/josaa.21.000113.

[22] F. T. Dullo, J. C. Tinguely, S. A. Solbø, and O. G. Hellesø, "Single-mode limit and bending losses for shallow Rib Si3N4 waveguides," *IEEE Photonics J.*, vol. 7, no. 1, 2015, doi: 10.1109/JPHOT.2014.2387252.

[23] R. Pregla, "The Method of Lines for the Analysis of Dielectric Waveguide Bends," *J. Light. Technol.*, vol. 14, no. 4, pp. 634–639, 1996.

[24] W. Bogaerts, S. K. Selvaraja, and S. Member, "Compact Single-Mode Silicon Hybrid Rib / Strip Waveguide With Adiabatic Bends," vol. 3, no. 3, 2011, doi: 10.1109/JPHOT.2011.2142931.

[25] R. N. Sheehan, S. Horne, and F. H. Peters, "The design of low-loss curved waveguides," *Opt. Quantum Electron.*, vol. 2009, no. August, pp. 1211–1218, 2009, doi: 10.1007/s11082-009-9329-7.

[26] Y. Qian, S. Kim, J. Song, G. P. Nordin, and J. Jiang, "Compact and low loss silicon-on-insulator rib waveguide 90° bend," *Opt. Express*, vol. 14, no. 13, p. 6020, 2006, doi: 10.1364/oe.14.006020.

[27] D. Yuan, Y. Dong, Y. Liu, and T. Li, "Design of a high-performance micro integrated surface plasmon resonance sensor based on silicon-on-insulator rib waveguide array," *Sensors (Switzerland)*, vol. 15, no. 7, pp. 17313–17328, 2015, doi: 10.3390/s150717313.

[28] R. A. Soref, J. Schmidtchen, and K. Petermann, "Large Single-Mode Rib Waveguides in GeSi-Si and Si-on-SiO2," *IEEE J. Quantum Electron.*, vol. 27, no. 8, pp. 1971–1974, 1991, doi: 10.1109/3.83406.

[29] H. Nejadriahi, A. Friedman, R. Sharma, S. Pappert, Y. Fainman, and P. Yu, "Thermo-optic properties of silicon-rich silicon nitride for on-chip applications," *Opt. Express*, vol. 28, no. 17, p. 24951, 2020, doi: 10.1364/oe.396969.

[30] A. W. Elshaari, I. E. Zadeh, K. D. Jöns, V. Zwiller, and W. Elshaari, "Thermo-Optic Characterization of Silicon Nitride Resonators for Cryogenic Photonic Circuits," doi: 10.1109/JPHOT.2016.2561622.

[31] G. Abbate, "The temperature dependence of the refractive index of water Electric Energy production View project," *Artic. J. Phys. D Appl. Phys.*, 2001, doi: 10.1088/0022-3727/11/8/007.